THE PENNSYLVANIA STATE UNIVERSITY
SCHREYER HONORS COLLEGE

SCHOOL OF SCIENCE

In Vitro Evaluation of Herbal Medicine on EGFR L858R Mutant Lung Cancer Cell Proliferation and Migration

TAYLOR M. ROMANIA
SPRING 2023

A thesis
submitted in partial fulfillment
of the requirements
for a baccalaureate degree in Biology
with honors in Biology

Reviewed and approved* by the following:

Jeremiah Keyes
Assistant Professor of Biochemistry and Molecular Biology
Thesis Supervisor

Michael Campbell
Distinguished Professor of Biology
Honors Adviser

* Electronic approvals are on file.

ABSTRACT

Epidermal growth factor receptor (EGFR) is a transmembrane receptor tyrosine kinase that, under normal functioning, undergoes conformational changes due to phosphorylation and participates in the cell's proliferation and maintenance. Upregulation of this protein is commonly observed in patients with non-small cell lung cancer, a disease responsible for a high percentage of cancer-related deaths in the United States. EGFR is also a protein successfully used as a target for cancer drug treatments. Recently, evidence has suggested herbal treatment options may be a successful alternative to chemotherapy, radiation, and other common cancer treatments. However, there is little molecular understanding of herbal therapies and limited studies on specific cancer mutations in response to the same treatments. This study aims to investigate cell proliferation and migration behavior within WT and L858R EGFR in response to herbal medical treatments as a potential treatment route.

TABLE OF CONTENTS

LIST OF FIGURES

ABBREVIATIONS

AIS: Adenocarcinoma in situ

Akt: Protein kinase B

CT: Computed tomography

EGFR: Epidermal growth factor receptor

JNK: c-Jun N-terminal kinases

MAPK: Mitogen-activated protein kinases

MIA: Minimally invasive adenocarcinoma

MRI: Magnetic resonance imaging

NSCLC: Non-small cell lung cancer

PET: Positron emission tomography

PTB: Phosphoserine binding domain

SCC: Squamous cell lung cancers

SCLC: Small cell lung cancer

SDM: Site directed mutagenesis

SH2: Src-homology 2

TCM: Traditional Chinese medicine

WT: Wildtype

ACKNOWLEDGEMENTS

I am grateful for the opportunity to formally express my appreciation to my esteemed supervisor, Dr. Jeremiah Keyes, for accepting me as his first undergraduate research assistant and guiding me through the perils of molecular biology and mammalian cell research. Throughout this journey, I have gained invaluable knowledge about both myself and the scientific process all while receiving unwavering support from Dr. Keyes. His mentorship has instilled in me the importance of embracing mistakes and learning through experimentation. I cannot thank him enough for the impact he has had on my personal and professional growth. I would also like to thank the Penn State Behrend biology department for their exceptional teaching style and passion for biology. Their contributions to my education have not gone unnoticed. Furthermore, I am deeply appreciative of Jared Toettcher at Princeton University for providing me with the stable pYtag NIH-3T3 cells that were essential for my experiment process and analysis. Finally, I would like to convey my deep gratitude to my family and friends for patiently listening to me ramble about research, despite not fully comprehending the processes. Their unconditional support has been a vital source of motivation throughout my undergraduate career, and I am immensely grateful for their unconditional encouragement.

Chapter 1 Epidermal Growth Factor Receptor

Epidermal Growth Factor (EGF) belongs to the EGFR family of RTKs, which includes proteins such as EGFR, ErbB2 (HER2/Neu), ErbB3 (HER3), and ErbB4 (HER4). These proteins share a similar structure: a large extracellular transmembrane region, an intracellular juxtamembrane region, a tyrosine kinase domain, and a C-terminal regulatory region [1]. Their crucial role in developing, growing, and maintaining multicellular organisms depends on forming homo- and heterodimers between receptors through ligand binding. Extensive research has focused on their role in the development of human cancer [2].

The Epidermal Growth Factor Receptor (EGFR) is widely known as a receptor tyrosine kinase (RTK) that plays a crucial role in the link between protein dysfunction and the development of cancer [3]. Human EGFR is an 1186 amino acid transmembrane glycoprotein with an NH2-terminal lobe composed primarily of β-strands, while the larger COOH- terminal lobe is formed entirely by α-helices. A cleft bordered by a glycine-rich nucleotide phosphate-binding loop (Gly695-Gly700), DFG motif (Asp831-Gly833), catalytic loop (Arg812-Asn818), and the A-loop (Asp831-Val852) separates these lobes [3].

1.1 EGFR Structure

The extracellular region of EGFR is 621 amino acids long and is divided into four domains (I – IV) known as L1, S1, L2, and S2. Domains I and III share 37% amino acid identity and contain ligand binding sites. Domain II forms homo- or heterodimers with analogous domains of family receptors and forms disulfide bonds with domain IV [4]. Domains I, II, and III

form the ligand binding head connected to the transmembrane helix through domain IV [5]. The intracellular domain consists of a juxtamembrane segment, a tyrosine kinase domain, and a C-terminal tail, totaling 542 amino acids. The structure of EGFR contains many tyrosine residues that allow the anchoring of intracellular proteins when phosphorylated [4] (Figure 1).

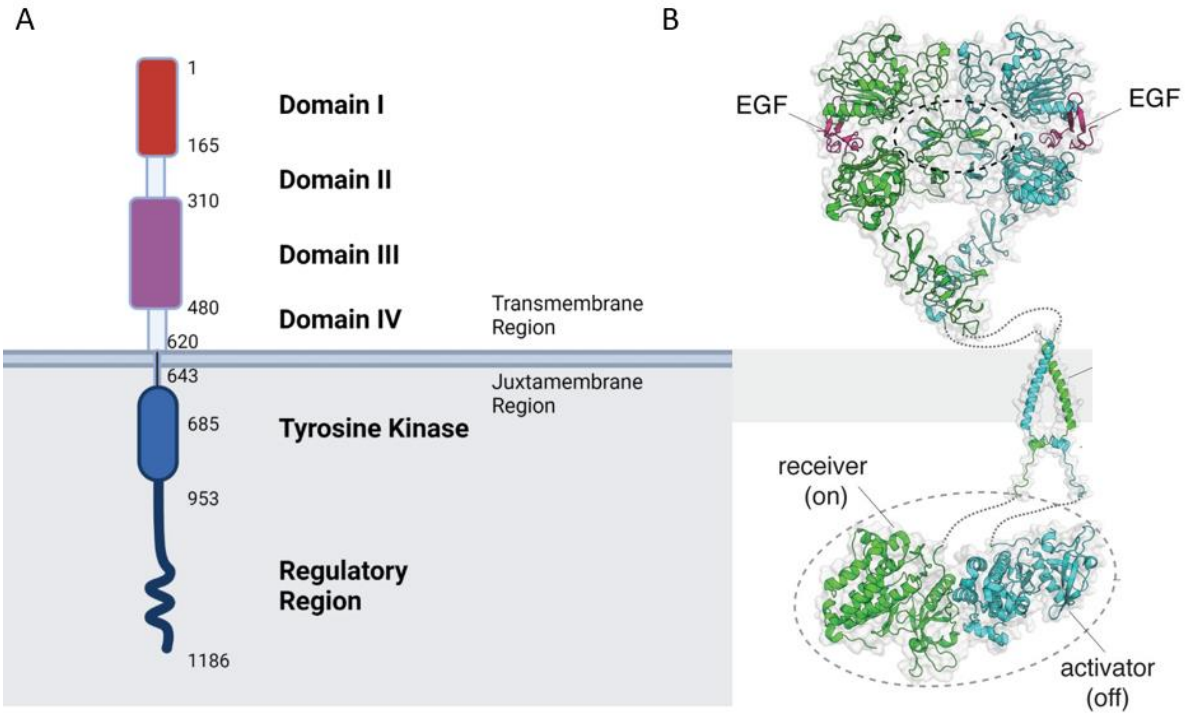

Figure 1: (A) Basic image of transmembrane EGFR monomer depicting the extracellular Domains I-IV and intracellular inactive tyrosine kinase and regulatory region (image created with bioRender.com) (B) Structure of EGFR dimer fragments: extracellular dimer bound to EGF (PDB code: 3NJP), transmembrane helix dimer (PDB code 2M20) and kinase domains (PDB code: 2GS6).

1.2 EGFR Function

EGFR activation depends on ligand-mediated homodimerization of EGFR receptors and heterodimerization of EGFR with other receptors. Subsequent autophosphorylation of

intracellular tyrosine kinases allows for the binding of signal transduction substrates such as phospholipases C-gamma I, GTPase-activation protein, and syp phosphotyrosine phosphatase [6]. Tyrosine kinase activation also triggers downstream signaling in pathways containing SH and PTB domains, including MAPK, Akt, and JNK, which influence DNA synthesis, cell proliferation, and differentiation [7] (Figure 2). EGFR inactivation requires receptor internalization and lysosomal degradation [6].

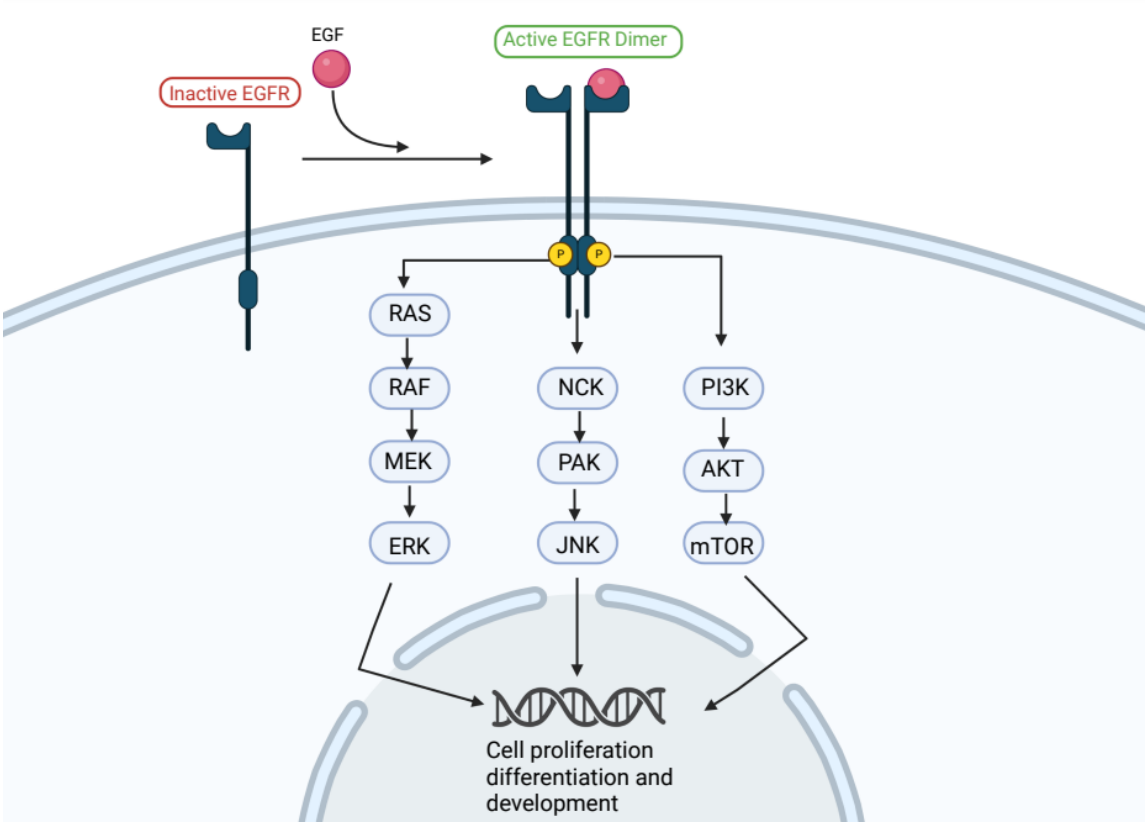

Figure 2: Downstream signaling of EGFR dimerization. EGFR selectively binds to EGFR receptors and triggers dimerization that activates pathways such as MAPK, Akt and, JNK. This activity influences cellular proliferation, DNA synthesis, and differentiation. (Image created with BioRender.com)

EGFR is typically expressed in epithelial, mesenchymal, and neurogenic tissues [7]. Its role in cell proliferation, differentiation, growth, migration, and apoptosis inhibition makes it a necessary protein for proper cellular functioning. Various cancers, including breast, head-and-neck, non-small-cell lung, bladder, colon, and pancreatic cancer, have been linked to EGFR protein dysfunction resulting from mutations in either the extracellular or intracellular regions [6]. Continuous research primarily focuses on EGFR crosstalk to understand how cancer develops resistance to inhibitory treatments with the goal of producing effective intervention, making it vital to understand for proper treatment of these disease.

Chapter 2 Cancer

Cancer is a destructive illness that originates from irregularities in the regulation of cellular growth mechanisms. Uncontrolled cell growth can lead to the formation of tumors within the lung parenchyma or bronchi, which can metastasize lead to death. Despite the significant advancements in cancer research and treatment, the complexity of this disease often requires a combination of treatments with uncertain outcomes depending on the cancer type and stage. Nevertheless, the global community of researchers, clinicians, and patients remains committed to developing effective treatments and, ideally, a cure.

Lung cancer developed through abnormal cell growth and lung tissue production is responsible for more than 25% of cancer-related deaths in the United States [8]. In the past few decades, lung cancer incidences have steadily risen due to smoking addictions [9]. With its highly invasive and rapidly metastasizing behavior, lung cancer is responsible for an estimated 350 deaths per day, or approximately 160,000 deaths each year [10]. Early detection and prompt treatment are crucial in improving the chances of survival for individuals diagnosed with lung cancer.

Lung cancer is categorized into four main classifications based on anatomical location: squamous cell lung cancers (SCC), adenocarcinomas, small cell lung cancer (SCLC), and large cell anaplastic carcinomas (NSCLC) [11]. While SCC and adenocarcinomas are considered subtypes of NSCLC, their distinct characteristics and diagnosis in different populations set them apart [12].

Squamous cell lung cancers (SCC) arise in the main bronchi of the lungs and account for 25-30% of all lung cancer cases [11]. This cancer is the most associated with a long history of smoking, as its development is directly linked to the keratinization of squamous cells lining the airway [13].

Adenocarcinomas are differentiated through their persistent tumor development in peripheral bronchi, accounting for 40% of lung cancer cases [11]. This type of lung cancer is further subdivided into adenocarcinoma in situ (AIS), minimally invasive adenocarcinoma (MIA), invasive adenocarcinoma, and variants of adenocarcinoma types. Unlike SCC, lung adenocarcinomas are commonly diagnosed in non-smokers, and their development is formed from granular structures in epithetical tissue lining the respiratory tract [14].

Small-cell lung cancer develops from hormonal imbalances within lung tissues that disseminate into submucosal lymphatic vessels [11]. Its notably fast proliferation rate makes it a candidate for early metastasis and poor ideal prognosis time [15].

Large-cell anaplastic carcinomas, also known as non-small cell lung cancer, are defined as tumors that invade the mediastinum [11]. NSCLC includes various lung cancers like the previously mentioned SCC and adenocarcinoma. Large cell carcinomas are further subdivided into adenosquamous carcinomas, sarcomatoid carcinomas, and non-small cell neuroendocrine tumors [16].

2.1 Diagnosis of Non-Small Cell Lung Cancers

The diagnosis of lung cancer is determined by analyzing histological factors and observing physical symptoms. In most cases, non-small cell lung cancer (NSCLC) is a heterogeneous disease that is histologically diagnosed through exclusion and typically exhibits

squamous, glandular, or neuroendocrine differentiation. Common intrathoracic effects of NSCLC include coughing, hemoptysis, chest pain, and dyspnea. About 20% of patients diagnosed with NSCLC may also present with bone metastasis, which can cause symptoms such as headache, vomiting, and visual deficits. Hypercalcemia and elevated alkaline phosphates are typical signs of bony metastasis, and further imaging studies such as CT, MRI, and PET scans are recommended. An official diagnosis of NSCLC requires a biopsy (for hisopathogenic and immunohistochemistry evaluation), chest and upper abdomen CT (to investigate metabolic disease), PET scans during treatment progress, and MRI (to assess brain metastasis) [16]. Additional biopsies, bronchoscopies, thoracentesis, and thoracoscopies are procedures used to gain a better understanding of the patient's cancer type, spread, and progression. This can be accompanied by biomarker testing to identify specific genes and proteins that are unique to the tumor for better treatment options [17].

During diagnosis, cancer staging is a crucial step that assists clinicians in determining the most appropriate treatment plan and helps facilitate communication of disease progression between treatment centers. The TNM-based staging system divides NSCLC diagnoses into four stages, ranging from stage I to stage IV. This system categorizes tumors based on three factors: T represents the size and extent of the primary tumor, N indicates the degree of regional lymph node involvement, and M signifies the presence or absence of metastatic spread [11].

The chances of survival and recovery are significantly higher when the disease is detected and treated at its early stages. To increase the chances of early detection, the American Cancer Society recommends routine screening for individuals that are at an increased risk of lung cancer. Therefore, it is essential for individuals to be aware of their risk factors for lung cancer

and to speak with their healthcare provider about the appropriate screening tests and options available [18].

2.2 The Role of EGFR L858R Mutation in Lung Cancer Development

Lung cancer is the result of the accumulation of genetic and epigenetic alterations. These changes disrupt the regulatory systems within the lung epithelium, leading to the formation of malignant tumors that invade and survive in lung tissues. [11]. Several factors contribute to the development of lung cancer, including extensive smoking histories and exposure to radiation, asbestos, and air pollution. Interestingly, there is no direct correlation between the number of cigarette packs smoked per year and the risk of lung cancer [9].

Studies suggest that gene-enzyme interactions that impact the detoxification of procarcinogens and DNA adduct formation play a significant role in determining an individual's susceptibility to tobacco-induced lung cancer [11]. The two most mutated oncogenic driver genes in lung cancer are EGFR and KRAS, which exist within a background of diverse putative tumor suppressor gene alterations [19]. Studies have confirmed that EGFRs are uniquely expressed in tumor tissues. In non-small cell lung cancer (NSCLC), certain mutations are known to contribute to the development of the disease. These include a short-frame deletion in exon 19 and point mutations in exon 21, such as the substitution of leucine with arginine at codon 858 (L858R) [7]. Overexpression of EGFR can lead to cell proliferation, angiogenesis, tumor invasion, and metastasis [20].

By focusing on specific genetic alterations that drive the development and progression of lung cancer, researchers can identify novel therapeutic targets and develop more effective treatment strategies.

Chapter 3 Treatments

3.1 Current Treatment Options for NSCLC Cancer Patients

There are many treatments used for lung cancer patients at all stages of progression. A comprehensive review of *Lung cancer: Biology and Treatment Options* published by Lemjabbar-Alaoui *et al.* in 2015 provides thorough discussion about this topic [11]. Key details are mentioned in this section.

Early stage (stage I and II) NSCLC is commonly treated with surgery. This allows patients to achieve long-term survival. In fact, the five-year survival rates after surgery are 60%-80% for stage I NSCLC and 30%-50% for stage II. Radiotherapy is a promising option for those who feel surgery is too great a risk or those who have a tumor that is inoperable. Stage II lung cancer patients have also shown improvement using platinum-based chemotherapy.

Unfortunately, most non-small cell lung cancer (NSCLC) diagnoses occur at advanced stages, which typically require a combination of treatment options for effective management. Stage III NSCLC accounts for 17% of all lung cancer diagnoses, and the available treatment options depend on various factors, including the tumor's location and the patient's overall health status. For patients with accessible tumors, surgery may be a viable option, but it is often followed by chemotherapy to increase the chances of success. For those with more aggressive stage III tumors, a combination of chemotherapy and radiotherapy may be necessary, either sequentially or concurrently.

Effective management of stage IV non-small cell lung cancer (NSCLC) involves a personalized approach tailored to individual patient needs and factors such as comorbidity, histology, and molecular genetic characteristics. A combination of therapies is often used in the

management of stage IV NSCLC, which may include external radiation, combination chemotherapy, laser therapy, or internal endoscopic radiation. First-line chemotherapy typically involves a combination of two cytotoxic drugs. These drugs target EGFR activation, including tyrosine kinase inhibitors such as erlotinib, gefitinib, and icotinib. Tyrosine kinase inhibitors are the preferred first-line therapy for patients with known EGFR activation mutations, especially those who are resistant to platinum therapy. If EGFR mutations are unknown, cytotoxic chemotherapy is usually the first-line treatment option. Recently, bevacizumab, an antibody that targets VEGF, has been added as a first-line doublet combination chemotherapy. However, it can only be given to patients without evidence of brain metastasis due to the risk of internal bleeding.

Second- and third-line therapies for patients with advanced NSCLC who have failed first-line platinum-based therapy include docetaxel, pemetrexed, erlotinib, and gefitinib. Pemetrexed has been shown to provide better outcomes for patients with lung adenocarcinoma, while docetaxel is more effective in patients with lung squamous cell carcinomas.

Recurring or relapsed NSCLC carries a heightened risk of spreading to all parts of the body. Treatment includes external palliative radiation therapy, cytotoxic chemotherapy, TKIs, and surgical resection for those who have already undergone chemotherapy. In a recent study, erlotinib has been shown to induce significant improvement in patient symptoms and survival when compared to standard second-line chemotherapy with docetaxel or pemetrexed. Overall, managing stage IV NSCLC requires careful consideration of each patient's unique circumstances to optimize outcomes. A personalized approach to treatment is essential to achieving the best possible outcomes for patients.

3.2 Alternative Treatment Options

In recent years, herbal treatment options have emerged as a successful alternative to conventional cancer treatments such as chemotherapy and radiation [21]. In March 2022, Sookyung Lee *et al* published a study documenting various successful herbal therapies in patients who were deemed "untreatable with conventional methods" [22]. Numerous cancer patients recorded considerable clinical outcomes, including stability in their disease progression or a significant improvement in their quality of life [22].

In China, studies have shown that small cell lung cancer (SCLC) patients use a combination of chemotherapy and Traditional Chinese Medicine (TCM) to enhance the effects of the first-line treatment [23]. The primary objective of herbal therapies is to reduce side effects resulting from conventional therapies, prevent cancer, and enhance the body's immune system [24]. TCM practitioners use a combination of psychological or physical approaches with herbal products to address health problems, including tai chi, acupuncture, and botanical dietary supplements [25]. Plants including *Platycodon grandiflorum* (Campanulaceae), *Morus alba* (Moraceae), *Prunus armeniaca* (Rosaceae), *Rhus verniciflua* (Anacardiaceae), *Perilla frutescens* (Labiatae), *Stemona japonica* (Stemonaceae), *Tussilago farfara* (Compositae), and *Draba nemorosa* (Brassicaceae) have been used to treat or supplement treatment of lung cancer [26].

There is limited understanding of the molecular mechanisms underlying these herbal therapies, and there are few studies on the cellular response of specific cancer mutations to the same treatments. To address this gap in knowledge, I propose to compare cell proliferation and migration behavior within WT and L858R (a common lung cancer mutation) in response to these herbal medical (TCM) treatments.

Chapter 4 Experiment Methodology

I propose to transfect cells with WT and mutated (L858R) EGFR and compare cell behavior when treated with herbal medications and the established TKIs erlotinib, gefitinib, and icotinib. To achieve this, I used mammalian cell culture, a valuable tool for studying cell and tissue behavior under desired conditions. To introduce specific DNA sequences into cells, I used a technique known as chemical transfection, which requires a vector with mammalian expression promotors to ensure proper expression. Insights into the role of the mutation in the response to herbal treatment could be determined by comparing the behavior of cell expression between WT and mutated EGFR. To do this, WT EGFR was subcloned into the mammalian expression vector pcDNA3.1, and the L858R mutation was created using site-directed mutagenesis.

This study utilized the well-established process of restriction enzyme cloning, which involved the extraction of WT EGFR from its current vector and its subsequent insertion into an empty pcDNA3.1 vector. PCR with customized primers was required to amplify the insert. The amplified WT sequence was subcloned into pcDNA3.1, followed by gel electrophoresis of cut and uncut plasmids for confirmation of the correct insert/vector. Once gel electrophoresis was complete, selected bands were purified, followed by ligation of the vector and insert. Finally, subcloning efficiency DH5α competent cells were used to transform the result of the ligation, and its colonies were purified through miniprep (Figure 3). The finished constructs were confirmed through a restriction digest check on an agarose gel, and apparent correct constructs were sent for confirmation with Sanger sequencing.

EGFR L858R was created using site-directed mutagenesis for the specific mutation of leucine to arginine at codon 858. PCR with custom primers was followed by KLD (kinase, ligase, and DLP) treatment, transformation, and purification through miniprep.

The finished plasmids can then be transfected into a mammalian cell line, treated with herbal extracts and their responses compared with microscopy. Cell behavior and EGFR activation are hypothesized to vary between herbal treatments compared to TKI-treated cells and control cells.

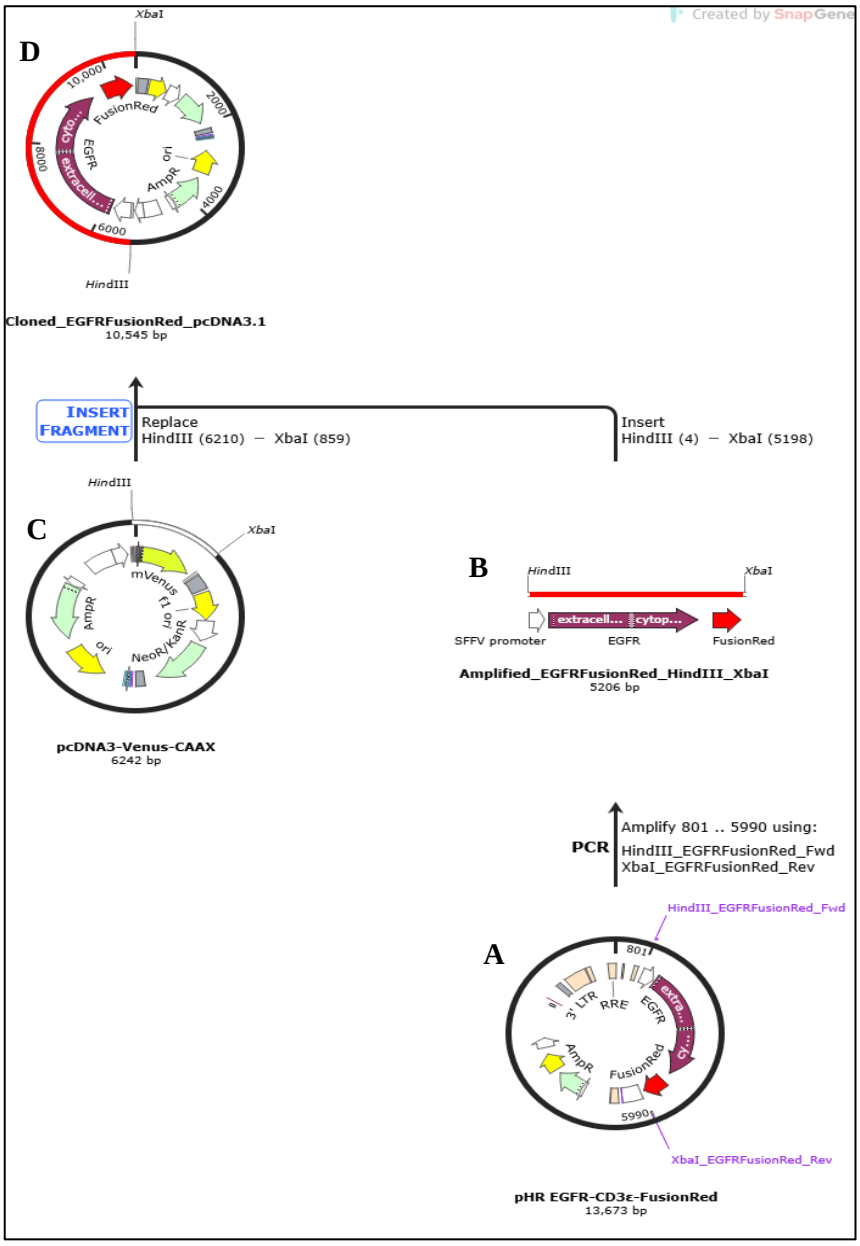

Figure 3: Overview of history for subcloning EGFR-CDƐ- Fusion Red into pcDNA3.1. (A) Original sequence of EGFR-CDƐ- Fusion Red in original pHR. Displayed on plasmid are custom forward and reserve primers with XbaI and HindIII restriction sites added (purple). (B) With these primers, the EGFR-CDƐ- Fusion Red sequence can be amplified using PCR. (C) At the same time, pcDNA3.1 can be digested with restriction enzymes to create an empty vector for ligation. (D) Ligation of amplified EGFR-CDƐ- Fusion Red with digested pcDNA3.1 creates "Cloned_ EGFR-CDƐ- Fusion Red_pcDNA3.1" plasmid.

This study also benefits from the use of pYtag NIH-3T3 cells, which were kindly provided by Jared E. Toettcher, Associate Professor of Molecular Biology at Princeton University. These cells were developed and tested by the Toettcher lab for monitoring specific RTK activity.

pYtags are RTKs modified with a tyrosine activation motif. When this motif is phosphorylated, it recruits a fluorescently labeled SH2 domain, enabling monitoring of the depletion of the fluorescent reporter from the cytosol and its local accumulation at the membrane during activation and SH2 recruitment (Figure 4). NIH-3T3 cells expressing Fusion Red fluorescent and iRFP-labeled ZtSH2 will be used to visualize these changes, providing a direct indication of EGFR activity. The use of pYtag NIH-3T3 cells is essential in the proposed experimental process. [21].

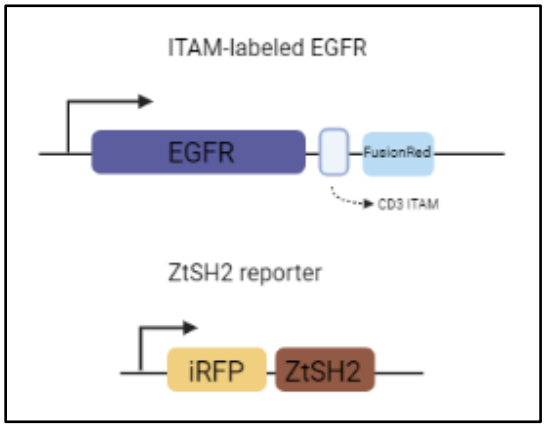

Figure 4 EGFR pYtag biosensor stably expressed in NIH-3T3 fibroblasts for detecting the activation of EGFR created by Jared Toettcher at Princeton University. Their approach uses ITAM selective recruitment of a specific SH2 domain upon EGFR activation. These NIH-3T3 express A) Fusion Red Fluorescent protein and B) iRFP-labeled ZtSH2 for direct indication of EGFR activity, measured by the depletion of iRFP from the cytosol.

This experiment's main objective was to optimize the treatment of herbal medications in mammalian cell line experiments to better understand the possible clinical implications for

patients with L585R-mutated lung cancer. Due to the unpredictable nature of molecular biology and cell culture, this goal was not fully achieved. However, this thesis provides a detailed outline for future researchers to build upon and further advance the understating in this area.

Chapter 5 Materials and Methods

4.1 Subcloning pHR EGFR-CDε- Fusion Red into Mammalian Expression Vector pcDNA3.1

A stab inoculation sample of pHR EGFR-CDε- Fusion Red was obtained from Addgene (https://www.addgene.org/188626/) and immediately streaked onto ampicillin agar plates for colony growth. One colony was inoculated in 2mL Ampicillin broth, and overnight at 37°C. After incubation, the broth was pelleted, and the DNA was purified by following the ZymoPURE Plasmid Midiprep vacuum protocol. The resulting purified DNA was quantified using the nanodrop (ng/µl).

The PCR reaction was completed using 10µl 5x reaction butter, 1µl of custom forward and reverse primers, 100ng PKAc template DNA, 0.5µl Onetaq DNA polymerase, and DI water to a final volume of 50µl. The PCR protocol involved an initial denaturation step at 94℃ for 30 seconds, followed by 30 cycles of denaturation at 94℃ for 30 seconds, annealing at 56℃ for 30 seconds, and extension at 72℃ for 4 minutes. A final extension step was carried out at 72℃ for 5 minutes to ensure the complete extension of the PCR product. The reaction was then held at 4℃ and stored at -20℃ for further use.

The recipient vector (pcDNA3.1) was prepared using a restriction digest. Three reaction tubes were labeled as uncut, double-cut, and single-cut. The double-cut tube contained 5µg of VenusCAAX-pcDNA3.1 vector DNA, 5µl of 10x Cutsmart buffer, 1µl of HindIII, 1µl of XbaI, and DI water to a final volume of 50µl. The single cut tube contained 500ng of venusCAAX-pcDNA3.1 vector DNA, 5µl of 10x Cutsmart buffer, 1µl of HindIII, and DI water to the final

volume of 50µl. The uncut tube contained 5µg of VenusCAAX-pcDNA3.1 without restriction enzymes. The reaction tubes were incubated at 37℃ for 15 minutes and stored at -20℃.

To confirm the success of the PCR reaction and restriction digest, gel electrophoresis was utilized. 10µl of loading dye was added to the pHR EGFR-CDε- Fusion Red PCR and VenusCAAX-pcDNA3.1 digest tubes, and a 1 kb ladder was loaded into the middle well of a 1% agarose gel containing 0.5x TAE buffer. The PCR products and digested DNA fragments were carefully loaded into separate wells of the gel, taking care to record the location of each reaction. The gel was then subjected to electrophoresis at 100V, which caused the DNA fragments to migrate toward the positively charged electrode and separate based on size.

The successful products of the pHR EGFR-CDε- Fusion Red PCR and the digestion of the VenusCAAX-pcDNA3.1 plasmid DNA were confirmed by the presence of bands at 4735bp and 5351bp, respectively. These bands were carefully cut and purified following the protocol outlined in the Zymoclean Gel DNA Recovery Kit. A nanodrop spectrophotometer was used to quantify the DNA concentration (ug/µl) of the gel purification.

The purified PCR product underwent an additional digest to create sticky ends for ligation. 10µl Cutsmart buffer, entire volume of pHR EGFR-CDε- Fusion Red PCR product, 1µl HindIII, 1µl XbaI, and DI water to the final volume of 50µl was added to a 1.5mL microcentrifuge tube. This was incubated at 37℃ for 15min followed by a 80℃ incubation for 20min.

NEBio Ligation Calculator (https://nebiocalculator.neb.com/#!/ligation) was used to calculate the amount of vector (pcDNA3.1) and insert (pHR EGFR-CDε- Fusion Red) needed for 3:1 and 5:1 ligation reaction. These reactions required 2µl 10x reaction buffer, 100ng vector

DNA, 3:1 or 5:1 insert volumes according to the website, 1µl T4 DNA ligase, and DI water to the final volume of 20µl. This reaction was incubated at room temperature overnight.

The subsequent transformation was conducted using 25µl DH5α cells and 5µl of each ligation reaction. A positive control was also prepared using 1µl pUC19. The tubes, now containing E. Coli and DNA, were incubated on ice for 25min, heat shocked at 42°C for 45 seconds, and then placed back on the ice for 1-2min. Sterile technique was used to add 500µl of SOC media to each tube, and they were placed in the shaker incubator at 37°C for 10min. Once incubation was complete, samples were spread on ampicillin plates and incubated overnight.

Incubation was followed by inoculation of 3 colonies per plate in 2mL ampicillin broth. DNA was purified the next day using ZymoPURE miniprep centrifugation protocol and the purified DNA was quantified on nanodrop (ng/µl).

500ng of the resulting purified DNA was used for a diagnostic restriction gel with 5µl 10x cut smart buffer, 1µl HindIII, 1µl xbaI, and DI water to the final volume of 50µl. These were run on a 1% gel with 0.5x TAE buffer and 1kb ladder at 100V. Ligation digests revealing an insert length of 891bp (~1000bp) indicate successful subcloning.

4.2 EGFR L858R Site-Directed Mutagenesis

Site-directed mutagenesis was performed using the NEB Q5 Site-Directed Mutagenesis Kit. Cloned EGFR-CDε-Fusion Red-pcDNA3.1 snapgene sequence was used to design primers for mutating Leucine to Arginine at codon 858. To perform the mutagenesis, 12.5µl of Q5 Hot Start HF 2x master mix, 1.25µl of 10µM forward and reverse custom primers, 25 ng of template DNA (successfully cloned and purified EGFR-CDε-Fusion Red-pcDNA3.1), and DI water to a final volume of 25µl was added to a PCR tube. The PCR protocol involved an initial

denaturation step at 98℃ for 30 seconds, followed by 25 cycles of denaturation at 98℃ for 10 seconds, annealing at 68℃ for 30 seconds, and extension at 72℃ for 5 minutes. A final extension step was performed at 72℃ for 2 minutes to ensure the complete extension of the PCR product and the reaction was then held at 4℃.

Subsequent KLD reaction was completed using 1µl PCR product, 5µl 2x KLD reaction buffer, 1µl 10x KLD enzyme mix, and DI water to the final volume of 6µl. This was incubated at room temperature for 5min and transformed using 25µl DH5α cells and 5µl EGFR L858R reaction. A positive control was also prepared using 1µl pUC19. Colony growth and inoculation were followed by DNA purification using the zymoPURE plasmid miniprep kit. Concentration was quantified using nanodrop (ng/µl).

4.3 Cell Culture

pYtag NIH-3T3 cells, obtained from Jared Toettcher at Princeton University, were cultured in dulbecco's modified eagle medium supplemented with 10% fetal bovine serum and 0.5% penicillin/streptomycin on T75 flasks. Cells were maintained at 37°C in a humidified incubator with a 5% CO_2 environment and passaged when confluency reached ~80% (approximately 3x per week).

4.4 Preparing Cells for Live-Cell Imaging

Two days before imaging, pYtag NIH-3T3 cells were seeded on a glass-bottom, 6-well plate at the density of 350,000 cells/well with a final volume of 2mL/well. Eighteen hours before imaging, cell media was replaced with serum-free media. Immediately before imaging, the serum-free media was replaced with imaging media consisting of phenol red-free DMEM.

4.5 Time-lapse Imaging and Treatment

Time-lapse imaging of pYtag NIH-3T3 cells was performed on a Nikon AXR live cell confocal microscope equipped with 405, 488, 560, and 640 nm lasers. Fusion Red and iRFP fluorescent protein visualization was accomplished using 561/650nm lasers at 40x objective during data acquisition. Initial imaging of cells was followed by 15min TKI pretreatment of 10μM Gefitinib, Erlotinib, Icotinib, and a combination of all TKIs to wells 2, 3, 4, and 6, respectively. 10μM DMSO was also added to well 1 to serve as the control. After 15min, 2 μl EGF was added to all wells and imaging continued for 10 min. At this time, 10μM gefitinib was added to well 4 and imaging resumed for 20min. Refer to Figure 5 for a detailed 6-well plate set-up.

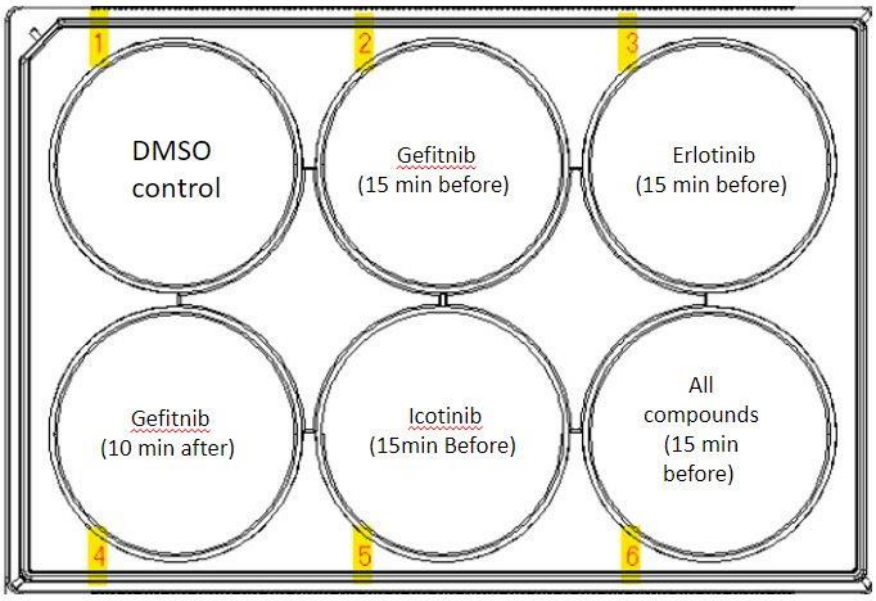

Figure 5: Illustration of the 6-well plate for pYtag NIH-3T3 live cell imaging using a Nikon AXR confocal microscope. Wells 2, 3, 5, and 6 were pretreated with TKIs 15min before EGF addition, while well 1 received DMSO as a control. 10min after EGF addition, posttreatment of gefitinib was added to well 4 and imaging continued for 20min

4.6 Analysis

The cell images were analyzed using Nikon software. After subtracting the background ROI, a threshold binary was applied to isolate the cytosolic regions of the cells. The binary was further refined using the binary editor. The mean intensity of the iRFP fluorescent protein was measured at each time point for each well. Finally, the activity of the EGFR RTK was determined using equation 1 as described by Toettcher *et al*.

$$activity_{RTK}(t) = -100 \cdot \left(\frac{I_{cyt}(t)}{I_{cyt,0}} - 1\right) \quad (1)$$

Where $I_{cyt}(t)$ is the cytosolic intensity of the timepoints after EGF treatment at and $I_{cyt,0}$ is the mean cytosolic intensity before EGF stimulation. To minimize data variation and ensure the reliability of experimental findings, it is preferable to conduct at least three biological replicates when collecting data.

Chapter 6 Results

6.1 Subcloning Results

Snapgene was used to create forward and reverse primers with HindIII and XbaI restriction sites, respectively: HindIII_GFR-CDε- Fusion Red forward primer sequence of CCTAAGCTTTTGGCAAGCTAGCTGC (Tm= 55°C) and XbaI GFR-CDε- Fusion Red reverse primer sequence of GCTTCTAGAGAGTCGCGGCCTCA (Tm= 57°C).

Initial streak from stab inoculation sample of pHR EGFR-CDε- Fusion Red resulted in colony formation (Figure 6) and the ampicillin broth became visibly cloudy after inoculation. Purified pHR EGFR-CDε- Fusion Red was quantified using nanodrop revealing a concentration of 464.6 ng/µl.

To initiate the PCR reaction, a DNA sample of 100ng was required. The calculated volume for amplified EGFR-CDε-Fusion Red, based on its concentration, was 0.2µl, which proved too small to pipette accurately. To address this challenge, the amplified EGFR-CDε-Fusion Red was diluted by a factor of 10, resulting in a concentration of 46.4 ng/µl. With the use of this modified concentration, it was determined that the volume for a 100ng PCR was 2.15µl.

For the EGFR-CDε-Fusion Red cloning experiment, we identified venusCAAX-pcDNA3.1 (2067 ng/µl) from our plasmid library as a suitable candidate for creating an empty pcDNA3.1 vector. 5µg of DNA was needed to initiate the digest reactions, based on the concentration of VenusCAAX-pcDNA3.1, 2.4 µl was needed.

After running the PCR and digest reactions on a gel, we observed a bold PCR band around 4000bp, a strong uncut band at ~6000bp, and a separated single-cut band primarily at ~6000bp. Additionally, separated double-cut bands were identified at ~10000bp and ~5000bp

(Figure 7). PCR and lower double-cut bands were carefully removed and purified. The nanodrop revealed gel purification concentrations to be 30.6 ng/µl for pcDNA3.1 vector and 81.8 ng/µl for EGFR-CDε-Fusion Red insert.

To ensure optimal ligation efficiency, we calculated the required amount of insert and vector for the 3:1 and 5:1 ligation reactions using the NEBio Ligation Calculator. Given an insert length of 4735bp and a vector length of 5351bp, the calculator suggested using 265.5 ng and 442.4 ng of insert, respectively, for the two ligation reactions with 100ng pcDNA3.1 vector. To account for dilution resulting from the PCR restriction digest (adjusted concentration at 21.26 ng/µl), we calculated that 12.4µl of EGFR-CDε-Fusion Red insert was needed for the 3:1 ligation reaction, while 20.8µl was required for the 5:1 ligation reaction.

After incubation, the transformed ligation reactions resulted in colony growth (Figure 8). After inoculating three colonies per plate and performing purification, we obtained the following 3:1 concentrations: colony A at 92.4ng/µl, colony B at 111.3ng/µl, and colony C at 166.4ng/µl. Similarly, we obtained the following the 5:1 concentrations: colony A at 123.0ng/µl, colony B at 73.6ng/µl, and colony C at 88.7ng/µl.

To verify the success of the ligation, a restriction digest was performed on 500ng of each reaction. For the 3:1 reactions, the calculated volumes for colonies A, B, and C were 2.8µl, 7.9µl, and 3.4µl, respectively. Similarly, for the 5:1 reactions, the calculated volumes were 6.5µl, 6.7µl, and 2.6µl for colonies A, B, and C, respectively. The samples were then run on a gel, which resulted in bold bands at ~5000bp and ~1000bp for all samples except EGFR-CDε-Fusion Red 3:1 colony B whose bands appeared ~5000bp and ~6000bp (Figure 9).

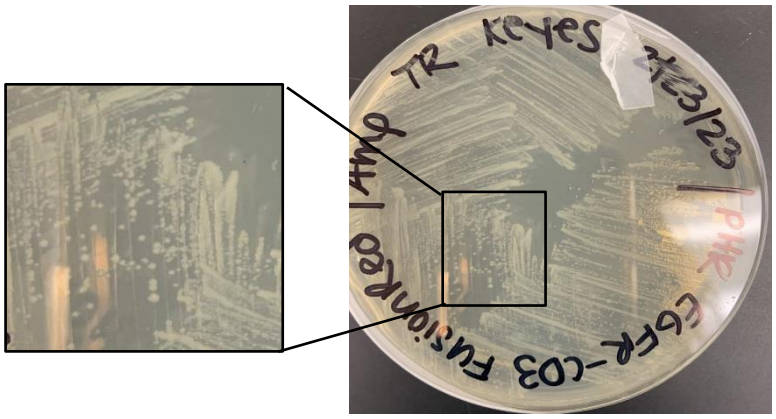

Figure 6: Results of initial streak from stab inoculation of pHR EGFR-CDε-Fusion Red obtained through addgene. Single colonies were inoculated and purified

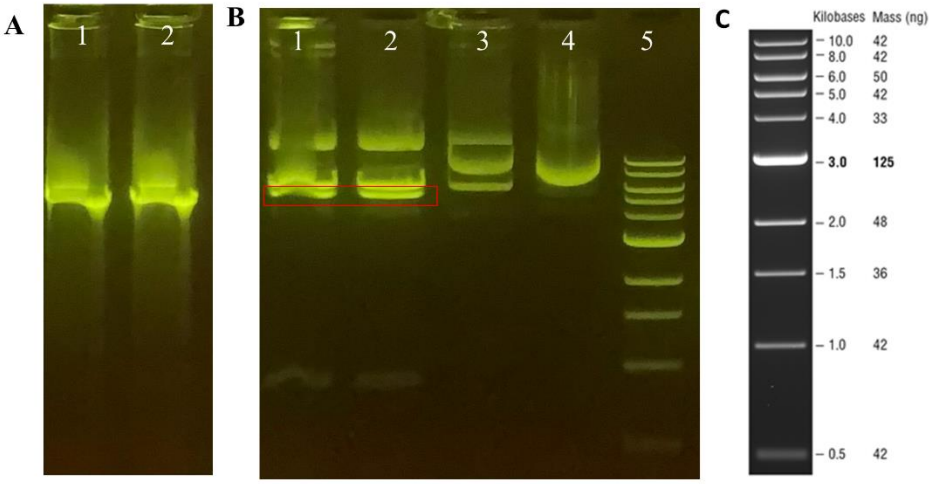

Figure 7: Gel electrophoresis of amplified EGFR-CDε-Fusion Red split between two wells (A1 and A2), double-cut pcDNA3.1 split between two wells (B1 and B2), single-cut pcDNA3.1 (B3), and uncut pcDNA3.1 (B4) on 1% gel with 1kb ladder (B5). PCR reaction bands at ~5000bp and lower double-cut at ~5000bp (red) were removed and purified.

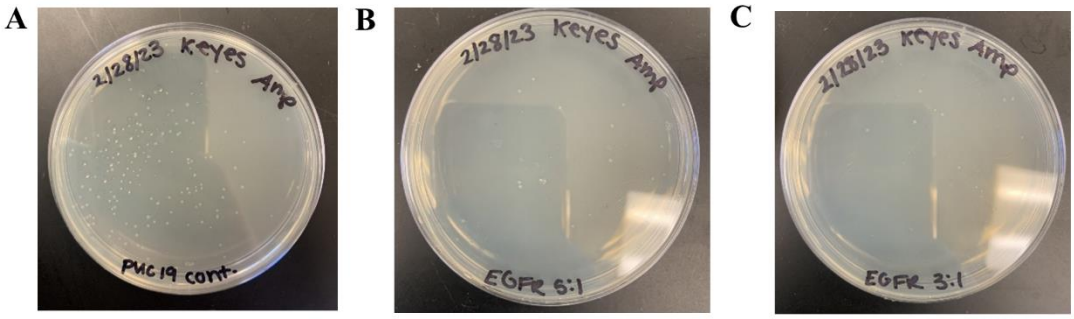

Figure 8: Result of transformation of 5:1 (B) and 3:1 (B) EGFR-CDε-Fusion Red- pcDNA3.1 ligation reactions on ampicillin plates. Colony growth was observed on the ligation plates, which was further supported by the colony growth seen on the pUC19 positive control (A). 3 colonies of each plate were inoculated and purified.

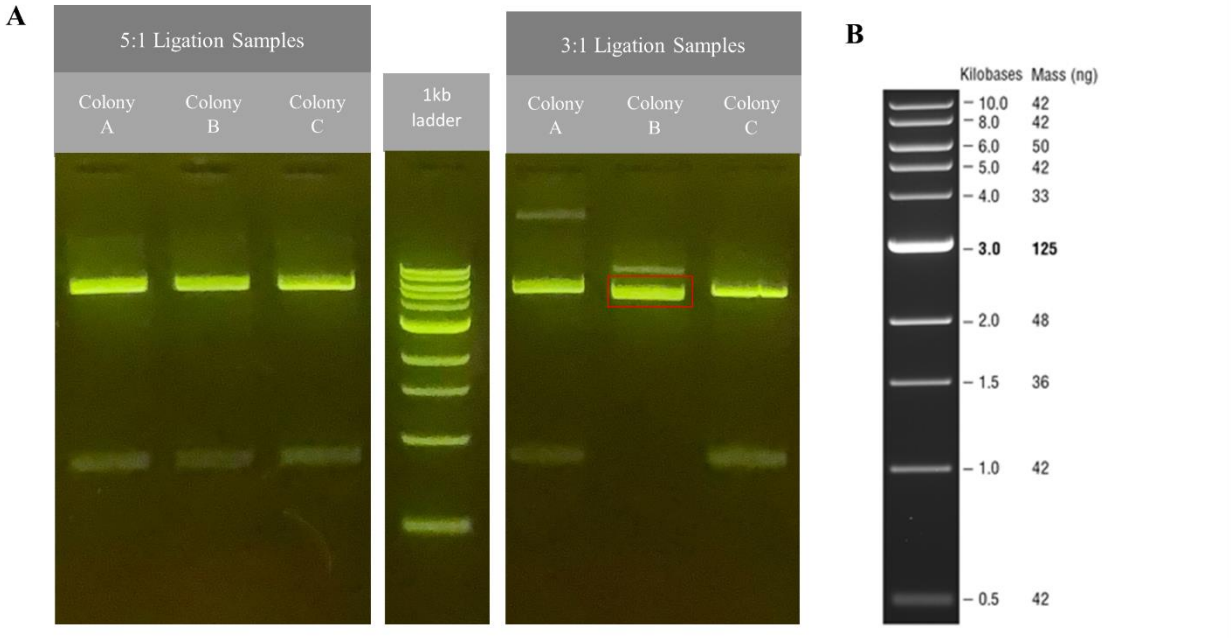

Figure 9: Restriction diagnostic gel check to confirm successful subcloning of EGFR-CDε-Fusion Red in pcDNA3.1 on 1% gel (A) with 1kb ladder (B). Gel image shows results of running 5:1 and 3:1 ligation reactions of digested and amplified EGFR-CDε-Fusion Red with digested pcDNA3.1. Results show bold bands at ~5000bp and ~1000bp for all samples except EGFR-CDε-Fusion Red 3:1 colony B whose bands appeared ~5000bp (red) and ~6000bp.

6.2 Site Directed Mutagenesis Results

Snapgene was used to create forward and reverse primers for the replacement of leucine with arginine at codon 858 using the subcloned EGFR-CDε-Fusion Red pcDNA3.1 plasmid sequence: EGFR L858R forward primer sequence of TCACAGATTTTGGGCGGGCAAACTGCTGGGTG (Tm= 69°C) and EGFR L858R reverse primer sequence of TCTTGCCATGCTGCGGTGTTTTCACCAGTACGTTC (Tm= 64°C).

Transformation of Site directed mutagenesis resulted in colony growth (Figure 10) and subsequent purification revealed EGFR L858R concentration of 148ng/µl.

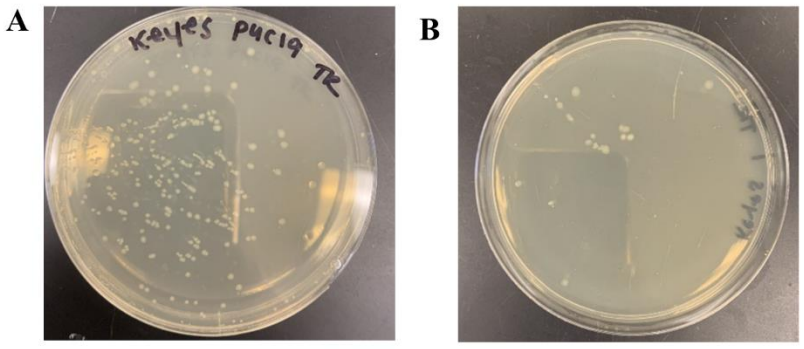

Figure 10: EGFR L858R site directed mutagenesis transformation (B) and pUC19 positive control (A) on ampicillin agar plates. One colony was inoculated and purified.

6.3 Live Cell Imaging Results and Analysis

During the experiment, pYtag NIH-3T3 cells underwent preliminary stages of cell death, as evidenced by their shrinking and becoming circular (Figure 11). Throughout the experiment, biosensors for EGFR activation and SH2 domain recruitment, EGFR Fusion Red and iRFP-ZtSH2 respectively, were visible in the images. Grayscale images of the DSMO control and All TKI wells revealed that the iRFP

biosensor was recruited to the plasma membrane following EGF stimulation (EGFR activation) (Figure 12).

Analysis focused on DMSO control and All TKI wells showed that EGFR activation in the DMSO control well spiked after EGF treatment and gradually decreased. In contrast, EGFR activation in the cells treated with all TKI showed low activation at TKI pretreatment, a spike after EGF stimulation, and a gradual increase in activity to the baseline level (Figure 13).

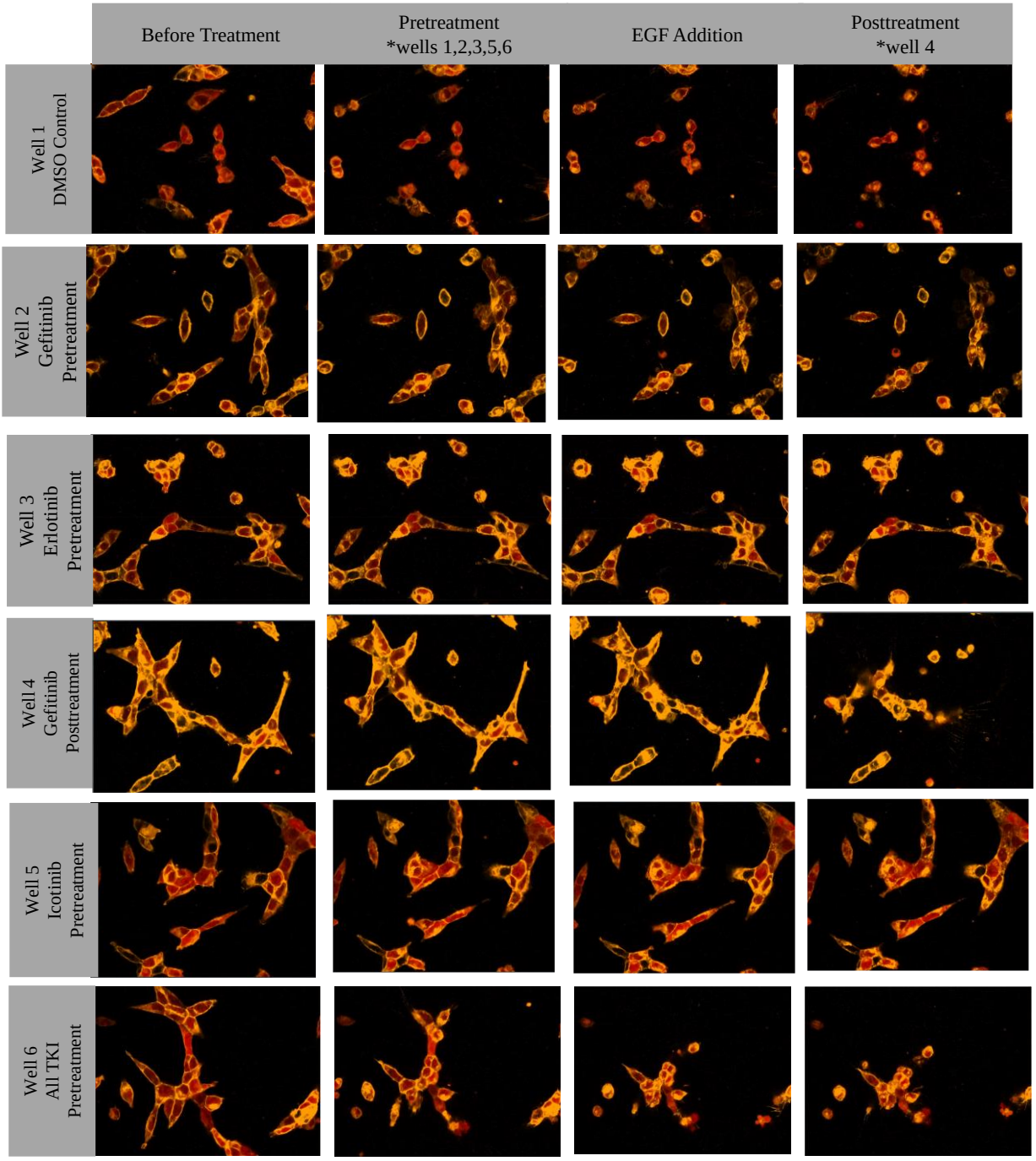

Figure 11: The cell images depicting the overlay of EGFR Fusion Red and iRFP-ZtSH2 biosensors were captured at various stages of the experiment for the treated wells. Specifically, the images were taken before treatment, after pretreatment with TKIs and DMSO in wells 1, 2, 3, 5, and 6, after EGF addition, and after post-treatment to well 1. Cells appear to shrink as experiment progressed.

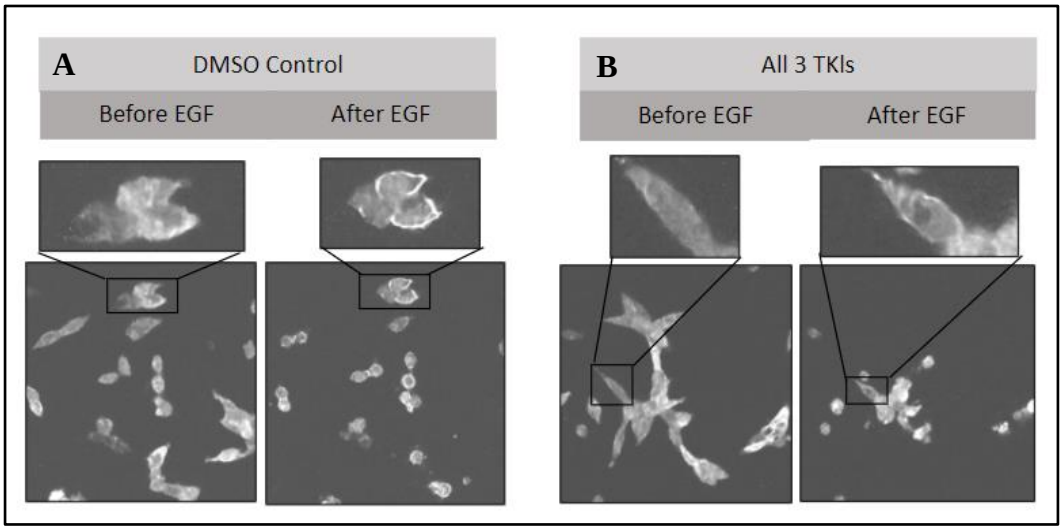

Figure 12: Grayscale images of iRFP-ZtSH2 biosensor in pYtag NIH-3T3 cells for DMSO control (A) and All TKI (B) wells. iRFP requirement of plasma membrane is visible after EGF treatment.

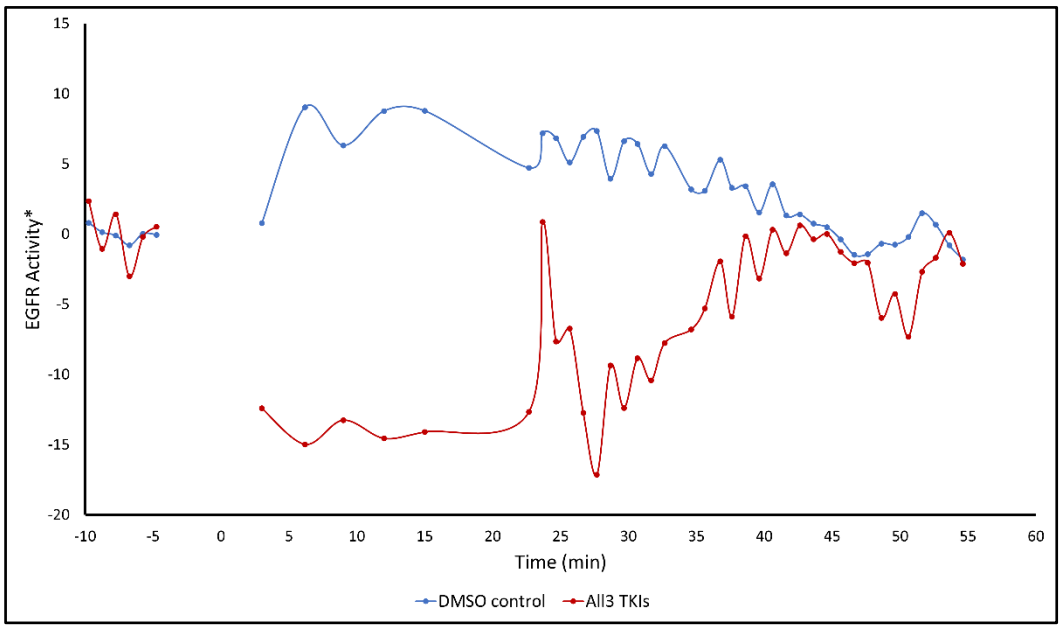

Figure 13: EGFR activation was calculated by comparing the normalized mean intensity of iRFP fluorescent protein values before and after EGF addition. The results showed that EGFR activation in the DMSO control well spiked after EGF treatment and gradually decreased. In contrast, the cells treated with all TKI showed low activation at TKI pretreatment (~5min - ~22min), followed by a spike in activation after EGF stimulation (~25min), and a gradual increase in activity to the baseline level.

Chapter 7 Discussion

7.1 EGFR-CDε-Fusion Red pcDNA3.1 Subcloning and EGFR L858R SDM

According to gel simulated on Snapgene, the expected band sizes for uncut pcDNA3.1 digest, single-cut digest and double-cut pcDNA3.1 digest were 6242bp (supercoiled), 6242bp (linearized) and 5351bp, respectively. Uncut (~ 6000bp) pcDNA3.1 displayed expected band size. Upon observation, the double-cut (bands at ~10000bp and ~5000bp) and single-cut (bands around ~6000bp) pcDNA3.1 were separated, leading to the conclusion that the double-cut sample contained partially digested pcDNA3.1. Taking this into consideration, the lower band at ~5000bp in the double-cut pcDNA3.1 sample corresponds to the desired empty vector. The PCR product EGFR-CDε-Fusion Red exhibited a band at ~5000bp that aligns with the predicted 4735bp band simulated on SnapGene.

Through snapgene we know that VenusCAAX insert size is expected at 891bp. Upon careful examination of the restriction digest gel, all ligation samples had a band at this size expect for EGFR-CDε-Fusion Red 3:1 ligation colony B with bands at ~6000bp and ~5000bp. It can be inferred that only this ligation sample was successful with the presence of the correct EGFR-CDε-Fusion Red insert and pcDNA3.1 vector, while the other samples still contained the VenusCAAX insert in pcDNA3.1.

The next step in preparation for mammalian cell transfection is to perform Sanger sequencing on both the EGFR-CDε-Fusion Red 3:1 ligation colony B and the EGFR L858R SDM result to verify the sequences of the WT and mutant plasmids.

7.2 Live Cell Imaging

The imaging results indicate that cells responded appropriately to the TKIs, as compared to the DMSO control. This suggests that the use of TKIs with pYtag NIH-3T3 cells is a reliable method for comparing cell behavior in future experiments.

7.3 Planning for Future Experiments

Unfortunately, due to the unpredictable nature of molecular and cell culture experiments, we encountered several issues that prevented us from collecting data on the effects of herbal medications. However, our work using pYtag NIH-3T3 cells to analyze EGFR activation has provided a reliable tool for such experiments. Future directions for this project include conducting replicate experiments using known TKIs (erlotinib, gefitinib, and icotinib) and herbal medicines (*Platycodon grandiflorum, Morus alba, Prunus armeniaca, Rhus verniciflua, Perilla frutescens, Stemona japonica, Tussilago farfara, and Draba nemorosa*) in a similar manner to the initial live cell imaging experiments that solely employed TKIs against a control.

Chapter 8 Conclusion

This experiment has provided a strong foundation and useful tool for comparing cell behavior between wild-type (WT) and mutated EGFR. By using pYag NIH-3T3 cells, comparing EGFR activity following treatment with TKIs and herbal medications, we can gain insight into the complex molecular mechanisms that drive cell behavior induced by mutant EGFR and its connection to lung cancer development.

BIBLIOGRAPHY

[1] Ferguson KM. Structure-based view of epidermal growth factor receptor regulation. Annu Rev Biophys. 2008; 37:353-73. doi: 10.1146/annurev.biophys.37.032807.125829. PMID: 18573086; PMCID: PMC2745238.

[2] Wieduwilt MJ, Moasser MM. The epidermal growth factor receptor family: biology driving targeted therapeutics. Cell Mol Life Sci. 2008 May;65(10):1566-84. doi: 10.1007/s00018-008-7440-8. PMID: 18259690; PMCID: PMC3060045.

[3] Stamos J, Sliwkowski MX, Eigenbrot C. Structure of the epidermal growth factor receptor kinase domain alone and in complex with a 4-anilinoquinazoline inhibitor. J Biol Chem. 2002 Nov 29;277(48):46265-72. doi: 10.1074/jbc.M207135200. Epub 2002 Aug 23. PMID: 12196540.

[4] Wee P, Wang Z. Epidermal Growth Factor Receptor Cell Proliferation Signaling Pathways. Cancers (Basel). 2017 May 17;9(5):52. doi: 10.3390/cancers9050052. PMID: 28513565; PMCID: PMC5447962.

[5] Yongjian HuangJana OgnjenovicDeepti KarandurKate MillerAlan MerkSriram SubramaniamJohn Kuriyan (2021) A molecular mechanism for the generation of ligand-dependent differential outputs by the epidermal growth factor receptor eLife 10: e73218.

[6] Murphrey MB, Quaim L, Varacallo M. Biochemistry, Epidermal Growth Factor Receptor. [Updated 2022 Sep 12]. In: StatPearls [Internet]. Treasure Island (FL): StatPearls Publishing; 2022 Jan-. Available from: https://www.ncbi.nlm.nih.gov/books/NBK482459/

[7] Bethune, G., Bethune, D., Ridgway, N., & Xu, Z. (2010). Epidermal growth factor receptor (EGFR) in lung cancer: an overview and update. Journal of thoracic disease, 2(1), 48–51.

[8] Lung cancer statistics: How common is lung cancer? American Cancer Society. (n.d.). Retrieved October 11, 2021, from https://www.cancer.org/cancer/lung-cancer/about/key-statistics.html.

[9] Siddiqui F, Vaqar S, Siddiqui AH. Lung Cancer. [Updated 2022 Dec 5]. In: StatPearls [Internet]. Treasure Island (FL): StatPearls Publishing; 2022 Jan-. Available from: https://www.ncbi.nlm.nih.gov/books/NBK482357/

[10] Siegel, RL, Miller, KD, Fuchs, HE, Jemal, A. Cancer statistics, 2022. CA Cancer J Clin. 2022. https://doi.org/10.3322/caac.21708

[11] Lemjabbar-Alaoui H, Hassan OU, Yang YW, Buchanan P. Lung cancer: Biology and treatment options. Biochim Biophys Acta. 2015 Dec;1856(2):189-210. doi: 10.1016/j.bbcan.2015.08.002. Epub 2015 Aug 19. PMID: 26297204; PMCID: PMC4663145.

[12] Basumallik N, Agarwal M. Small Cell Lung Cancer. [Updated 2022 Jul 12]. In: StatPearls [Internet]. Treasure Island (FL): StatPearls Publishing; 2022 Jan-. Available from: https://www.ncbi.nlm.nih.gov/books/NBK482458/

[13] Sabbula BR, Gasalberti DP, Anjum F. Squamous Cell Lung Cancer. [Updated 2022 Nov 5]. In: StatPearls [Internet]. Treasure Island (FL): StatPearls Publishing; 2022 Jan-. Available from: https://www.ncbi.nlm.nih.gov/books/NBK564510/

[14] Myers DJ, Wallen JM. Lung Adenocarcinoma. [Updated 2022 Jun 21]. In: StatPearls [Internet]. Treasure Island (FL): StatPearls Publishing; 2022 Jan-. Available from: https://www.ncbi.nlm.nih.gov/books/NBK519578/

[15] Rudin CM, Brambilla E, Faivre-Finn C, Sage J. Small-cell lung cancer. Nat Rev Dis Primers. 2021 Jan 14;7(1):3. doi: 10.1038/s41572-020-00235-0. PMID: 33446664; PMCID: PMC8177722.

[16] Clark SB, Alsubait S. Non-Small Cell Lung Cancer. [Updated 2022 Sep 5]. In: StatPearls [Internet]. Treasure Island (FL): StatPearls Publishing; 2022 Jan-. Available from: https://www.ncbi.nlm.nih.gov/books/NBK562307/

[17] Collins LG, Haines C, Perkel R, Enck RE. Lung cancer: diagnosis and management. Am Fam Physician. 2007 Jan 1;75(1):56-63. PMID: 17225705.

[18] *Lung cancer early detection: Lung cancer screening*. Lung Cancer Early Detection | Lung Cancer Screening. (n.d.). Retrieved March 30, 2023, from https://www.cancer.org/cancer/lung-cancer/detection-diagnosis-staging/detection.html

[19] Foggetti G, Li C, Cai H, Hellyer JA, Lin WY, Ayeni D, Hastings K, Choi J, Wurtz A, Andrejka L, Maghini DG, Rashleigh N, Levy S, Homer R, Gettinger SN, Diehn M, Wakelee HA, Petrov DA, Winslow MM, Politi K. Genetic Determinants of EGFR-Driven Lung Cancer Growth and Therapeutic Response *In Vivo*. Cancer Discov. 2021 Jul;11(7):1736-1753. doi: 10.1158/2159-8290.CD-20-1385. Epub 2021 Mar 11. PMID: 33707235; PMCID: PMC8530463.

[20] Hong W, Wu Q, Zhang J, Zhou Y. Prognostic value of EGFR 19-del and 21-L858R mutations in patients with non-small cell lung cancer. Oncol Lett. 2019 Oct;18(4):3887-3895. doi: 10.3892/ol.2019.10715. Epub 2019 Aug 6. PMID: 31516600; PMCID: PMC6732961.

[21] Farahani PE, Yang X, Mesev EV, et al. pYtags enable spatiotemporal measurements of receptor tyrosine kinase signaling in living cells. bioRxiv; 2022. DOI: 10.1101/2022.08.13.503850.

[22] Sookyung Lee, Sora Park, Ha Yeon Lee, Hyeonjin Jeon, Soomin Lee, Seongheon Choi, Wankyu Eo, A potential treatment option for advanced non-small cell lung cancer: Three cases, EXPLORE, 2022, ISSN 1550-8307, https://doi.org/10.1016/j.explore.2022.04.001. (https://www.sciencedirect.com/science/article/pii/S155083072200043X)

[23] Mi X, Zhang X, He S, Zhang Z, Qi R, Jiang J, Chen S, Zheng H, Hua B. Chinese herbal medicine for small cell lung cancer patients: A protocol for a systematic review and meta-analysis. Medicine (Baltimore). 2020 Dec 24;99(52):e23746. doi: 10.1097/MD.0000000000023746. PMID: 33350758; PMCID: PMC7769348.

[24] Tavakoli J, Miar S, Majid Zadehzare M, Akbari H. Evaluation of effectiveness of herbal medication in cancer care: a review study. Iran J Cancer Prev. 2012 Summer;5(3):144-56. PMID: 25628834; PMCID: PMC4294537.

[25] U.S. Department of Health and Human Services. (n.d.). Traditional Chinese medicine: What you need to know. National Center for Complementary and Integrative Health. Retrieved April 2, 2023, from https://www.nccih.nih.gov/health/traditional-chinese-medicine-what-you-need-to-know

[26] Yin SY, Wei WC, Jian FY, Yang NS. Therapeutic applications of herbal medicines for cancer patients. Evid Based Complement Alternat Med. 2013;2013:302426. doi: 10.1155/2013/302426. Epub 2013 Jul 11. PMID: 23956768; PMCID: PMC3727181.

ACADEMIC VITA

Education and Honors

Bachelor of Science in Biology
Minor in Biochemistry and Molecular Biology
Schreyer Honors College
Pennsylvania State University, *Erie, PA*
Expected Graduation: May 2023 | Dean's List: *Fall 2019 - Present*

Academic Awards

Academic Excellence in Biology Award *Spring 2023*
Penn State Behrend 2022 Undergraduate Research Grant *May – August 2022*
Behrend Honors Certificate *May 2021*
Penn State Behrend 2021 Undergraduate Research Grant *May – August 2021*
Aaron Meehl Biology Award – Outstanding Rising Junior *Spring 2021*

Work and Research Experience

Pharmacy Technician |Select Medical Healthcare Company – Erie, PA *July 2021 –Present*

- Collaborated with pharmacists to identify and resolve medication-related issues, ensuring accurate and timely delivery of medications to patients.
- Consistently delivered medications to nurses in a timely and accurate manner, contributing to efficient patient care and positive patient experiences.
- Perform appropriate protocols for IV compound and medication preparation.

Research Assistant | Pennsylvania State University – Erie, PA *October 2020 - Present*

- Proficient in basic molecular and biochemical techniques, including PCR, transformation, restriction enzyme cloning, and DNA purification, gained through conducting research.
- Experienced in mammalian cell culture and microscopy, with experience conducting research in this area.
- Knowledgeable in communicating the completion of protocols on various web platforms, ensuring accurate and timely documentation of research progress.
- Contributed to multiple research projects, including designing experiments, collecting, and analyzing data, and presenting findings to team members.

Belonging@Behrend | Pennsylvania State University – Erie, PA
CORE Intern *January 2021- May 2021*

- Provided coaching and guidance to mentors on curriculum topics such as trauma training, healthy habits, setting boundaries, and addressing questions.
- Collaborated with other interns to enhance the connection between mentors and mentees.
- Actively participated in meetings with supervisors to address program challenges and provide recommendations for improvement.

Mentor *September – December 2020*

- Facilitated a successful transition from high school to college for first-year students.
- Provided leadership for two weekly Zoom classes, teaching essential skills such as study habits, resilience, and imposter syndrome.
- Collaborated with co-mentor to delegate curriculum leadership and ensure the effective delivery of material.

Leadership Involvement

Lion Ambassadors, Internal Affairs Committee Head *Spring 2021 - Present*

- Participated in club-run activities and service events to represent our school community
- Organized and tracked club member participation to ensure proper involvement.

Science Ambassadors, Treasurer, and President *Spring 2021- Present*

- Represented the school and science field by volunteering and organizing STEM events.

Welcome Week, Guide, and Leader *August 2021, 2022*

- Coordinated and directed teams of volunteers to facilitate the move-in process for incoming first-year students, ensuring a welcoming and organized first day for new students.